“Il n’y a pas hors du schème”

Determination of PM Flux Linkage Based on Minimum Saliency Tracking for PM-SyR Machines Without Rotor Movement

Paolo Pescetto, *Member, IEEE,* and Gianmario Pellegrino, *Senior Member, IEEE,*

***Abstract*—Permanent Magnet assisted Synchronous Reluctance (PM-SyR) motors often present relevant magnetic saturation, especially if overload capability is exploited. The knowledge of current-to-flux relationship is mandatory for proper motor control, and it becomes even more critical in case of sensorless applications. Reliable standstill self-commissioning tests have been recently developed for Synchronous Reluctance (SyR) motors without producing rotor movement. This procedure can be extended to PM-SyR motors, but, being at standstill, it does not retrieve the flux contribution related to the PMs. This paper integrates the identification of the flux characteristics including a novel test for estimating the PM flux linkage, obtaining the complete magnetic characteristic of the PM-SyR motor. The identification session is performed at standstill and without a position transducer, independently of the mechanical load being connected or not. Such conditions are considered the most demanding for self-commissioning tests. The machine is first excited with a proper sequence of bipolar high voltage pulses to determine its current dependent flux components. Then, the estimate of PM flux linkage is retrieved at standstill by evaluating the local saliency along the negative *q*-axis. The proposed method is supported by detailed finite element analysis and experimentally verified on two PM-SyR motor prototypes, confirming the accuracy of the PM flux linkage estimate.**

***Index Terms*—Self Commissioning, PM Flux, PMSM, PM Synchronous Reluctance Machines, Magnetic Model Identification, Flux Maps.**

I. Introduction

The industrial interest in Synchronous Reluctance (SyR) motors is recently growing in a wide number of applications, mostly because of their high efficiency and competitive torque per volume ratio respect to the Induction Motors (IM), their good overload capabilities and their generally lower cost respect to PM Synchronous Machines (PMSM). Moreover, the high anisotropy of SyR motors makes them suitable for low speed sensorless control, which commonly exploits saliency based algorithms [1]–[3]. The main drawbacks of SyR machines are their generally limited flux weakening capability and low power factor, which leads to inverter oversize. The addition of small amount of PM into the flux barriers, resulting in a PM-SyR motor, considerably improves both the power factor and the speed power curve at high speed [4], with limited impact on the cost of the drive.

One major disadvantage of both SyR and PM-SyR machines is their highly non-linear magnetic characteristic (flux maps), presenting direct and cross saturation effects [5], [6], as can be seen in Fig. 1. Accurate knowledge of the flux maps is often required for control calibration [7]–[9], especially in sensorless applications [8], [10]–[13]. The standard methods for inductance measurement of synchronous machines [14], [15] require a dedicated test rig and off-line identification of each new machine. Recently, several self-commissioning techniques were proposed [16]–[20], normally requiring a rotary encoder, or the rotor to be locked or free to rotate at sufficiently high speed. These requirements may not be respected in industrial environment, thus limiting the applicability of the methods like [17], [20]. In [21], [22] accurate standstill self-identification techniques were proposed, able to identify the complete magnetic model of SyR motors at standstill without locking the rotor and not implying position transducers, which are considered the most demanding conditions. The method was further improved in [23], increasing the measurement domain and demonstrating that the obtained flux maps are reliable for sensorless control of SyR machines.

Standstill commissioning tests usually do not include the PM flux linkage contribution λ_{pm}, necessary, as an example,

P. Pescetto and G. Pellegrino are with the Department of Energy Galileo Ferraris, Politecnico di Torino, Torino,Italy e-mail: paolo.pescetto@polito.it, gianmario.pellegrino@polito.it

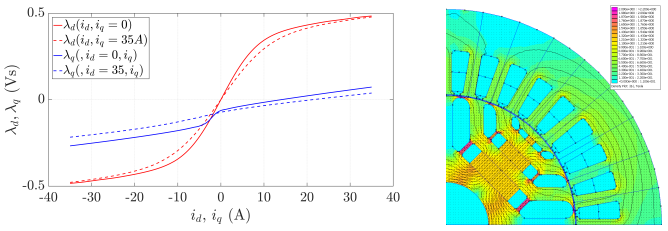

(a)

(b)

Fig. 1. (a) Reference flux maps of one of the machines under test (Mot_1) and (b) cross-section of the other one (Mot_2).

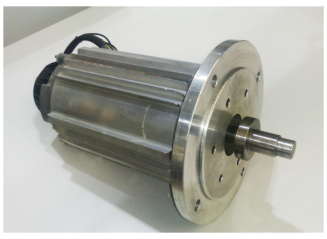

(a)

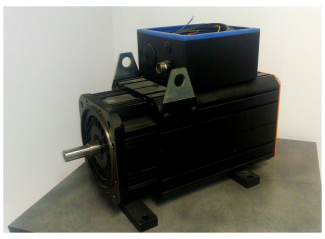

(b)

Fig. 2. Pictures of the two PM-SyR machines experimentally tested: (a) Mot_1, (b) Mot_2.

TABLE I
RATINGS OF THE PM-SYR MOTORS UNDER TEST.

	Mot_1	Mot_2
Nominal current [A]	28	22.2
Nominal dc-link voltage [V]	360	310
Pole pairs	2	2
Nominal torque [Nm]	27	19
$T_{\rm PM}/T_{\rm n}$ **(%)**	10.5	34.2
Nominal speed [rpm]	2500	2500
Maximum speed [rpm]	10000	9000
Nominal peak power [kW]	10	7

to retrieve the MTPA trajectory or calibrating a flux observer [24]. In most cases, $\lambda_{\rm pm}$ is evaluated by measuring the back-EMF voltage while the shaft rotates at open windings. Such operation requires a prime mover and voltage transducers and it is necessarily performed off-line. Evaluating $\lambda_{\rm pm}$ at standstill is necessary, for example, when the load is already connected to the drive or if the rotor is locked. Some commissioning algorithms retrieve the PM polarity only [25], but not the amplitude of $\lambda_{\rm pm}$. A feasible solution is to online adapt the estimated $\lambda_{\rm pm}$ during operation, as for example in [26], [27], but increasing the complexity of the motor control and anyway requiring an initial estimate. Quasi-standstill methods for $\lambda_{\rm pm}$ measurement were proposed in [28]–[30]. Anyway, [28] needs a position transducer and a calibrated speed loop, so it is not compatible with sensorless applications, while [29], [30] imply free-shaft conditions and minor rotor movements.

This work exploits the self-commissioning technique of [22] for measuring the armature flux maps of PM-SyR motors, adding a novel solution for evaluating the PM flux linkage. The test is based on the evaluation of local incremental anisotropy along the PM axis. Differently from any previous solutions, the test is completely standstill. The proposed self-commissioning technique is sensorless, meaning that none of the identification stages needs a position transducer, with the load either connected or not.

The proposed technique is experimentally validated on two PM-SyR motor prototypes, called Mot_1 and Mot_2 (shown in Fig. 2), whose specifications are reported in Table I. Moreover, the FEA models of four other PM-SyR machines are exploited in the Appendix to justify the validity of the test sequence.

This paper represents an extension of its conference version [31]. The substantial improvements include:

- theoretical investigation of the minimum saliency locus of PM-SyR machines;
- deep validation using Finite Element Analysis (FEA), evaluating the influence of PM quantity and structural ribs thickness on the accuracy of $\lambda_{\rm pm}$ estimation;
- experimental validation on a second PM-SyR machine.

II. MODEL OF PM-SYR MACHINES

This section shortly reviews the basic model of PM-SyR machines. The synchronous dq coordinates will be adopted, being the d-axis the direction of minimum reluctance on the rotor. The PM flux linkage is aligned with the negative q-axis.

A. Fundamental Model

The fundamental component of stator voltage is given by:

$$\begin{cases} v_{\rm d} = R_{\rm s} i_{\rm d} + \frac{{\rm d}\lambda_{\rm d}}{{\rm d}t} - \omega\lambda_{\rm q} \\ v_{\rm q} = R_{\rm s} i_{\rm q} + \frac{{\rm d}\lambda_{\rm q}}{{\rm d}t} + \omega\lambda_{\rm d} \end{cases} \tag{1}$$

The flux linkage components follow a non-linear relationship, commonly called flux maps:

$$\begin{cases} \lambda_{\rm d} = \lambda_{\rm d}\left(i_{\rm d}, i_{\rm q}\right) \\ \lambda_{\rm q} = \lambda_{\rm q}\left(i_{\rm d}, i_{\rm q}\right) \end{cases} \tag{2}$$

The d axis is the direction of maximum inductance. The reference flux maps of the two tested prototypes Mot_1 and Mot_2 were experimentally evaluated in a dedicated test according to [15]. The flux maps of Mot_1 are reported in Fig. 1(a).

B. High Frequency Model

If the motor is excited with a High Frequency (HF) signal, the resistive voltage drop and motional terms in (1) at such frequency become small respect to the flux derivative. Therefore, (1) reduces to:

$$\begin{cases} v_{\rm dh} \approx \frac{{\rm d}\lambda_{\rm d}}{{\rm d}t} \\ v_{\rm qh} \approx \frac{{\rm d}\lambda_{\rm q}}{{\rm d}t} \end{cases} \tag{3}$$

where the subscript h stands for the HF component. It is useful to define the differential inductances, which determine the relationship between current and flux derivative:

$$l_{\rm d} = \frac{\partial\lambda_{\rm d}}{\partial i_{\rm d}} \qquad\qquad l_{\rm q} = \frac{\partial\lambda_{\rm q}}{\partial i_{\rm q}} \tag{4}$$

$$\begin{cases} \lambda_{\rm dh} \approx l_{\rm d} i_{\rm dh} \\ \lambda_{\rm qh} \approx l_{\rm q} i_{\rm qh} \end{cases} \tag{5}$$

C. PM and Armature Flux Linkage Breakdown

The $\lambda_{\rm q}(i_{\rm d}, i_{\rm q})$ characteristic of PM-SyR machines includes the PM flux linkage component $\lambda_{\rm pm}$. As proposed in [29], the $\lambda_{\rm q}(i_{\rm d}, i_{\rm q})$ characteristic is split into the current dependent term $\lambda_{\rm q0}(i_{\rm d}, i_{\rm q})$, or armature flux, and the negative offset $\lambda_{\rm pm}$:

$$\lambda_{\rm q}\left(i_{\rm d}, i_{\rm q}\right) = \lambda_{\rm q0}\left(i_{\rm d}, i_{\rm q}\right) - \lambda_{\rm pm} \tag{6}$$

where $\lambda_{\rm q0}$ is null for $(i_{\rm d}, i_{\rm q}) = (0, 0)$ and $\lambda_{\rm pm}$ is a constant value, function of the PM temperature. Otherwise said, $\lambda_{\rm pm}$ is the flux linkage in q axis when the current is null, by definition:

$$\lambda_{\rm q}\left(i_{\rm d} = 0, i_{\rm q} = 0\right) = -\lambda_{\rm pm} \tag{7}$$

III. Commissioning of the Armature Flux Maps

The method in [22] is adopted here for evaluating the current-dependent terms of the flux maps (λ_d and λ_q0) of the PM-SyR machine, also called armature flux.

At first, a standard sensorless HF injection technique is adopted to evaluate the initial rotor position $\hat{\theta}_0$. It is assumed that the rotor does not move during the test, so $\hat{\theta}_0$ is used to define the dq axes during the complete commissioning stage.

Then, a 3-step procedure is adopted. At the first stage (**test #1**), the d-axis is excited with bipolar square-wave voltage. The amplitude of the applied voltage is on the same order of magnitude of the motor rated voltage (e.g. 220 V), while its polarity is reversed when i_d overcomes a defined threshold value, according to a symmetric hysteresis mechanism. Meanwhile, $v_\mathrm{q} = 0$. Since the d-axis only is excited, the produced torque is alternated and not excessive, being the PM torque component only of a PM-SyR machine.

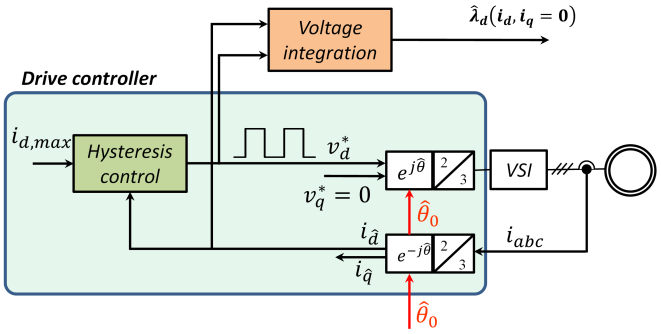

Fig. 3. Control block diagram for test #1.

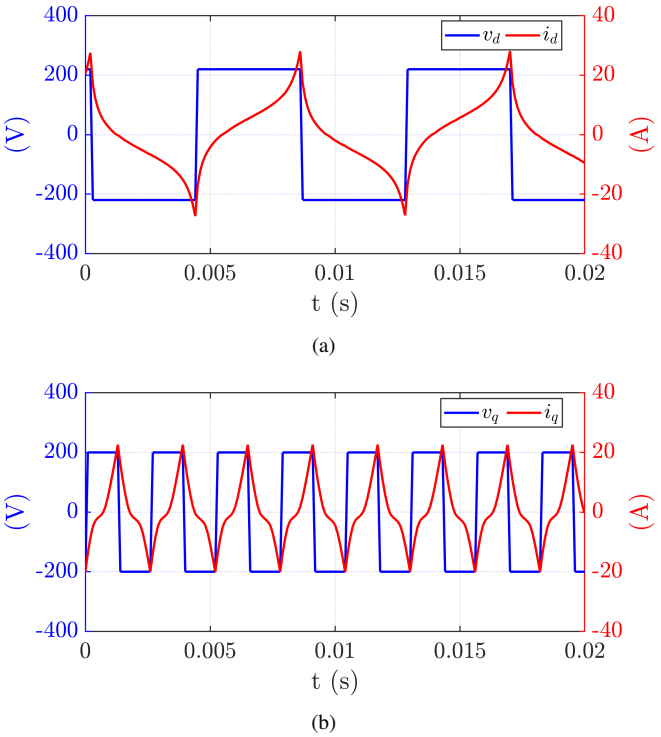

Fig. 4. Current and voltage waveforms during test #1 (Mot_1).

Therefore, the motor does not move, whatever the mechanical load. Fig. 3 shows the motor control block diagram for test #1. The self-saturation flux characteristic in d axis $\lambda_\mathrm{d}(i_\mathrm{d}, i_\mathrm{q} = 0)$ is retrieved from EMF integration:

$$\lambda_\mathrm{d} = \int \left(v_\mathrm{d} - \hat{R}_\mathrm{s} i_\mathrm{d} \right) \mathrm{d}t \tag{8}$$

where $\hat{R}_\mathrm{s}$ is the estimated stator resistance and v_d is estimated from inverter commands, after compensation of inverter voltage drop.

The **test #2** is dual to the first one, but the q axis is excited with a hysteresis based square-wave voltage while $v_\mathrm{d} = 0$. The curve $\lambda_\mathrm{q}(i_\mathrm{d} = 0, i_\mathrm{q})$ is obtained, again from EMF integration:

$$\lambda_\mathrm{q} = \int \left(v_\mathrm{q} - \hat{R}_\mathrm{s} i_\mathrm{q} \right) \mathrm{d}t \tag{9}$$

Again, one axis only is excited, but in this case the excitation is in the direction of the PM. Therefore, in principle torque is not produced. However, this test is less stable than the previous one, since eventual inaccuracy in the estimation of $\hat{\theta}_0$ may result in drifting from the initial position. In this case, the test would fail. For this reason, test #2 can be augmented (if necessary) with online position tracking [23].

Finally, in **test #3** the two axes are simultaneously excited to evaluate the cross-coupling flux linkage. Eq. (8),(9) are simultaneously adopted to retrieve the flux maps $\boldsymbol{\lambda}_\mathrm{dq}(\boldsymbol{i}_\mathrm{dq})$ over the entire dq plane. A more detailed description of the test sequence can be found in [22]. Anyway, this test will not be presented here, since the main contribution of this work is retrieving λ_pm without any rotor movement, and the proposed procedure is immune from cross-coupling effect. It should be noted that the cross-saturation effect in PM-SyR machines is very similar to the SyR case, already addressed in [22]. Therefore, from here on the cross-coupling will be neglected.

The voltage and current waveforms obtained while testing the machine Mot_1 are reported in Fig. 4.

A. Discussion

This identification procedure was initially formulated for SyR machines and now adopted for the PM-SyR case. These motors present a $\lambda_\mathrm{d}(i_\mathrm{d})$ characteristic similar to an equivalent SyR machine, but, differently from the SyR case, the PM produce transient torque during test #1, which may move the rotor from its initial position, as said. Anyway, the torque reversal happens at considerably high frequency (30÷50 Hz), so that the rotor may slightly vibrate in pure free shaft conditions, but without considerably moving from its initial position. If necessary, also this test can be augmented with HF voltage injection for online position tracking, as addressed in [23].

As for test #2, this only provides the armature flux component $\lambda_\mathrm{q0}(i_\mathrm{q})$, without the PM contribution. Fig. 5 and 6 show the results of the two tests on the two PM-SyR motors experimentally tested (Mot_1 and Mot_2). The initial state of the integrator in (8),(9) is appropriately set to force $\lambda_\mathrm{d}(i_\mathrm{d} = 0) = 0$ and $\lambda_\mathrm{q0}(i_\mathrm{q} = 0) = 0$. As can be seen, in both cases the estimated $\lambda_\mathrm{d}(i_\mathrm{d})$ curve is very close to the reference

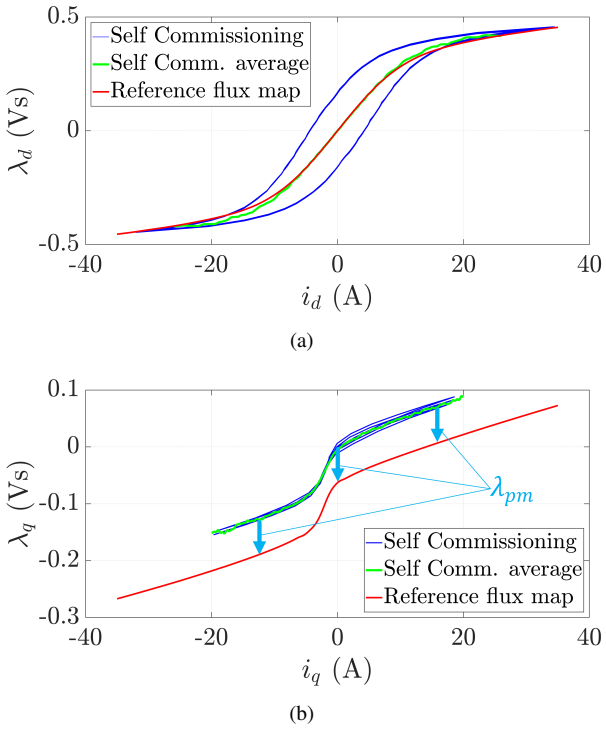

Fig. 5. Experimental results of standstill commissioning on d- and q-axes armature flux for Mot_1.

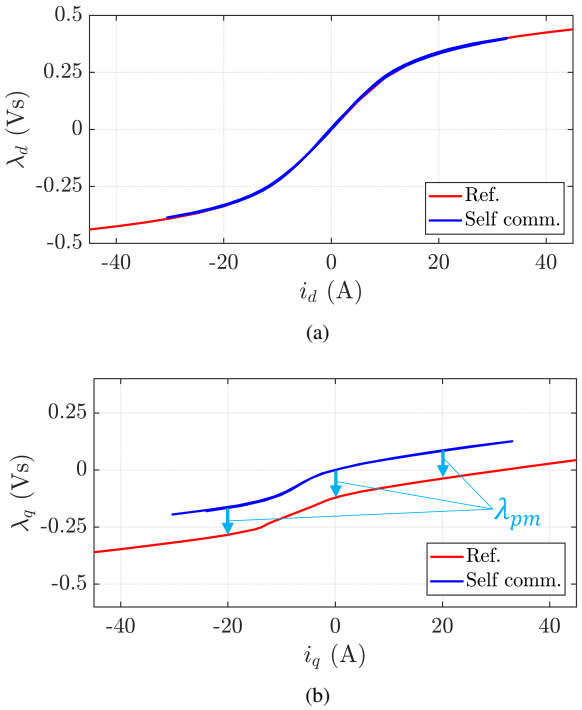

Fig. 6. Experimental results of standstill commissioning on d- and q-axes armature flux for Mot_2.

trajectory, while $\lambda_{q0}(i_q)$ presents the correct shape, shifted by the quantity λ_{pm}. A dedicated additional test is needed to retrieve λ_{pm}, as proposed in the next sections.

IV. PM Flux Identification at Standstill

The self-commissioning paradigm requires the identification to be at free shaft and standstill, avoiding to measure the open circuit back-EMF. A feasible solution proposed in [29] is to exploit the Zero Torque Locus (ZTL), defined as the trajectory in the dq plane where the torque is null, out of the q-axis. Along this trajectory, the reluctance torque is counteracted by the PM torque component. Considering the well known formulation for the electro-mechanical torque:

$$T = \frac{3}{2} p \left(\lambda_{\mathrm{d}} i_{\mathrm{q}} - \lambda_{\mathrm{q}} i_{\mathrm{d}} \right) = 0 \tag{10}$$

therefore, based on (6):

$$\left(\lambda_{\mathrm{q0}} - \lambda_{\mathrm{pm}} \right) i_{\mathrm{d}} = \lambda_{\mathrm{d}} i_{\mathrm{q}} \tag{11}$$

This equation presents two possible solutions. The first is $i_{\mathrm{d}} = 0$ and so $\lambda_{\mathrm{d}} = 0$, which means the current vector is aligned with the magnets (q-axis). This solution is not useful for determining λ_{pm}. The second solution, which can be extracted considering $i_{\mathrm{d}} \neq 0$, is the ZTL, highlighted in blue in Fig. 7(a). Along this trajectory, the PM and reluctance effects are even, resulting in zero torque:

$$\lambda_{\mathrm{pm}} = \lambda_{\mathrm{q0}} - \frac{\lambda_{\mathrm{d}} i_{\mathrm{q}}}{i_{\mathrm{d}}} \tag{12}$$

This last equation could be used in any point of this line to obtain an estimation of λ_{pm}. However, it is convenient to apply (12) to the singular point $(i_{\mathrm{d}} = 0, i_{\mathrm{q}} = i_{\mathrm{qT0}})$, defined as the intercept between the ZTL and the q axis:

$$\begin{aligned} \lambda_{\mathrm{pm}} &= \lim_{(i_{\mathrm{d}}, i_{\mathrm{q}}) \to (0, i_{\mathrm{qT0}})} \left(\lambda_{\mathrm{q0}} \left(i_{\mathrm{q}} \right) - \frac{\lambda_{\mathrm{d}} i_{\mathrm{q}}}{i_{\mathrm{d}}} \right) \\ &= \lambda_{\mathrm{q0}} \left(i_{\mathrm{qT0}} \right) - L_{\mathrm{d}} i_{\mathrm{qT0}} \end{aligned} \tag{13}$$

Fig. 7(b) explains the application of (13). Since (13) refers to the condition $i_{\mathrm{d}} \to 0$, the apparent inductance $L_{\mathrm{d}} = \frac{\lambda_{\mathrm{d}}}{i_{\mathrm{d}}}|_{i_{\mathrm{d}} \to 0}$ is basically the inductance in the linear region of the $\lambda_{\mathrm{d}}(i_{\mathrm{d}})$ curve. Therefore, a reliable value of L_{d} can be conveniently evaluated from the results of test #1 for low i_{d}, while $\lambda_{\mathrm{q0}}\left(i_{\mathrm{q}}\right)$ is obtained from test #2. Therefore, at this point of the procedure the only missing parameter to evaluate λ_{pm} is the key current value i_{qT0}. Reference [29] proposed to evaluate i_{qT0} from a sequence of rotor alignments at freeshaft. A novel procedure is defined here based on machine local saliency, performed at standstill whatever the mechanical load.

V. Analysis of the $\lambda_{\mathrm{q}}(i_{\mathrm{q}})$ Characteristic

Before describing the local saliency based method, the shape of $\lambda_{\mathrm{q}}(i_{\mathrm{q}})$ curve must be analyzed. As can be seen in Fig. 5(b), this curve is almost linear for every current value except a restricted area at negative i_{q} where a sharp rate change occurs. This strong inductance variation is related to de-saturation of the rotor structural ribs.

For null or positive i_{q} the ribs are saturated and the differential inductance l_{q} is almost constant. At negative current, the armature and PM flux components have opposite effect on the ribs, so for sufficiently high negative i_{q} the saturation is lost.

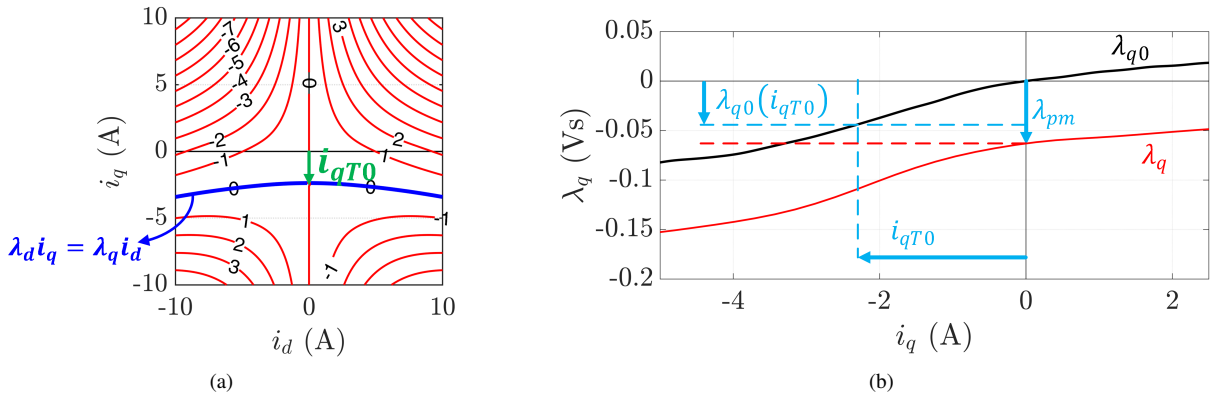

(a) (b)

Fig. 7. (a) Representation of zero torque locus and (b) zoom of q axis flux characteristic (Mot_1).

In this condition, the incremental q inductance is extremely higher than in the rest of the $i_{\rm q}$ domain, and both $l_{\rm q}$ and $\lambda_{\rm q0}$ curves show a sharp variation. In this region, $l_{\rm q}$ is close to $l_{\rm d}$, so the saliency drastically drops. The $i_{\rm q}$ value corresponding to the inflection point, i.e. maximum slope of the $\lambda_{\rm q}$ curve and so maximum $l_{\rm q}$, will be called $i'_{\rm qT0}$. If the negative $i_{\rm q}$ is further increased, the flux contribution due to $i_{\rm q}$ overcomes $\lambda_{\rm pm}$, thus saturating the ribs in the opposite direction respect to the one imposed by the PM. Beyond this point, the curve is again linear.

For better explaining the concept, Fig. 8 represents the magnetic density plot of one pole of the Mot_1 PM-SyR protorype, obtained with accurate FEA. The FEA simulation is executed three times. In Fig. 8(a), the stator current is zero, and the PM saturate the structural ribs, leading to $l_{\rm d} >> l_{\rm q}$. In Fig. 8(b), the minimum saliency point of the q axis was simulated, i.e. ($i_{\rm d}$=0,$i_{\rm q} = i'_{\rm qT0}$). As can be seen, in this condition the structural ribs are not saturated, and so the magnetic flux can flow almost linearly either in d and q direction. As a result, the reluctance along d and q axes is nearly the same and so $l_{\rm d} \approx l_{\rm q}$. In Fig. 8(c) the negative $i_{\rm q}$ was further increased ($i_{\rm q}$=-7 A). As can be noted, the ribs are saturated again, so $l_{\rm d} >> l_{\rm q}$, but differently from Fig. 8(a) the saturation is due to the current instead of the PM, so the magnetic induction in the ribs has opposite sign.

VI. Experimental Determination of $i_{\rm qT0}$ and $\lambda_{\rm pm}$ Based on Minimum Saliency

The basic assumption behind the method proposed here is that the current $i_{\rm qT0}$ is nearly equal to the current corresponding to maximum $l_{\rm q}$, i.e. $i'_{\rm qT0}$. In other words, the curve $\lambda_{\rm q}(i_{\rm q})$ presents its maximum slope approximately at $\lambda_{\rm q}(i_{\rm qT0})$. It must be noted that this condition also corresponds to the minimum local saliency along the q-axis.

To demonstrate this assumption is rather critical analytically, since in that area the machine behavior is strongly non-linear. A physical explanation is given in the Appendix, supported by FEA analysis.

If $i_{\rm qT0} \approx i'_{\rm qT0}$ is assumed, the latter can be used in place of $i_{\rm qT0}$ in (13) for evaluating $\lambda_{\rm pm}$:

$$\lambda_{\rm pm} \approx \lambda_{\rm q0}\left(i'_{\rm qT0}\right) - L_{\rm d} i'_{\rm qT0} \tag{14}$$

Therefore, a dedicated test is proposed to experimentally evaluate $i'_{\rm qT0}$, as described in the following.

A. Saliency Evaluation Test

Again, the rotor position does not change during the test so $\hat{\theta}_0$ is adopted for dq frame definition.

The motor control diagram is reported in Fig. 9. A fundamental DC current vector is forced in negative q-axis through a simple PI based current control loop ($i^*_{\rm d} = 0$). At the meantime, a HF rotating voltage component $\boldsymbol{v}_{\rm dqh}$ is superimposed to the fundamental excitation:

$$\begin{cases} v_{\rm dh} = u_{\rm c} cos\left(\omega_{\rm c} t\right) \\ v_{\rm qh} = u_{\rm c} sin\left(\omega_{\rm c} t\right) \end{cases} \tag{15}$$

where $u_{\rm c}$ and $\omega_{\rm c}$ are the amplitude and angular frequency of the injected voltage. According to the HF model described in Section II-B, the HF current response can be evaluated as:

$$\begin{cases} i_{\rm dh} = \frac{u_{\rm c}}{\omega_{\rm c} l_{\rm d}} sin\left(\omega_{\rm c} t\right) \\ i_{\rm qh} = -\frac{u_{\rm c}}{\omega_{\rm c} l_{\rm q}} cos\left(\omega_{\rm c} t\right) \end{cases} \tag{16}$$

So, the HF current response describes an elliptic curve, and the eccentricity of the ellipse indicates the local saliency.

It should be noted that the PI regulators in d and q axes impose the DC reference values of $i^*_{\rm d}$ and $i^*_{\rm q}$, without dynamic requirements other than converging to the setpoint after a reasonable amount of time (e.g. 5 ms). Therefore, the calibration of the PI is not critical and can be easily computed based on the results of Tests #1 and #2. The goal of the Band-Stop Filter (BSF), centered in $\omega_{\rm c}$, is to remove the HF component from the current feedback, avoiding a distortion of the injected rotating voltage due to the PI controller.

The reference fundamental current vector is slowly moved along negative q-axis, permitting to evaluate the local anisotropy and thus finding $i'_{\rm qT0}$. This test was repeated on the two prototypes experimentally tested. Fig. 10 shows the current trajectories in the dq plane (Mot_1) in some key points and defines the quantities $\Delta i_{\rm d}$, $\Delta i_{\rm q}$, Δi_{min} and Δi_{max}.

It should be noted that in this test the motor is excited along the PM direction. Therefore, even at free shaft and/or in case of inaccurate initial position estimation $\hat{\theta}_0$ the test cannot provoke any rotor movement.

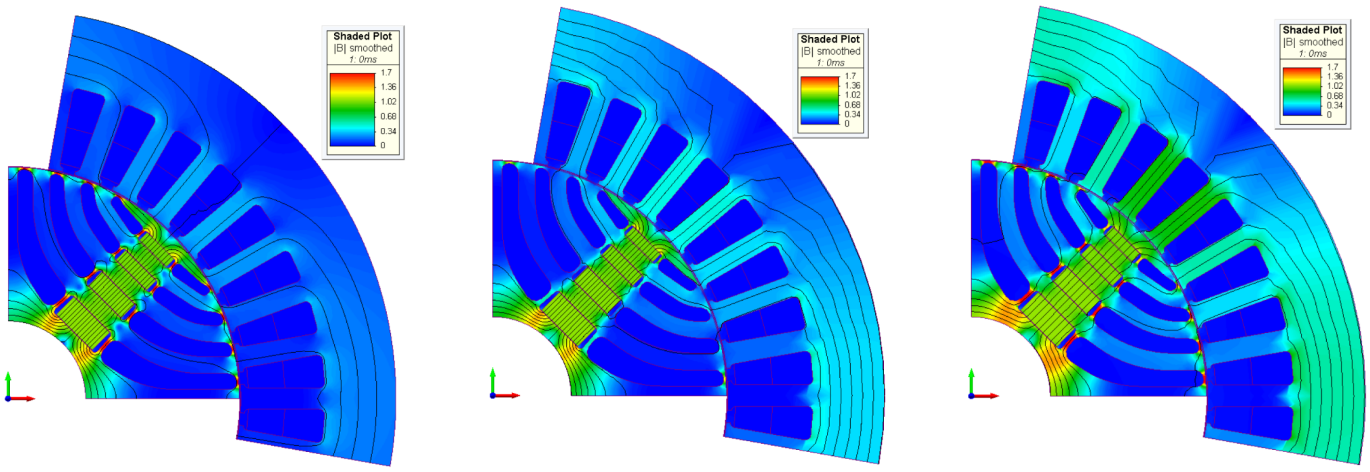

(a) (b) (c)

Fig. 8. FEA for one of the PM-SyR machines under test (Mot_1). (a) zero current (i_d=0,i_q=0); (b) minimum saliency point (i_d=0,$i_\mathrm{q} = i'_{\mathrm{qT0}}$); (c) below the knee ($i_\mathrm{d}$=0,$i_\mathrm{q}$=-7 A).

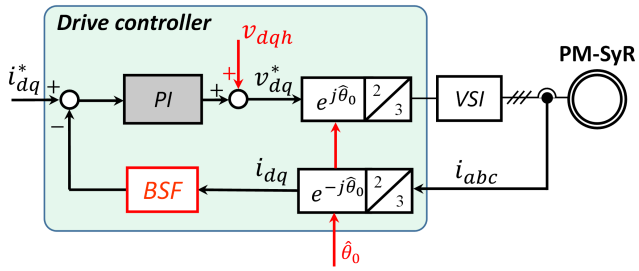

Fig. 9. Block diagram for local saliency evaluation.

TABLE II
COMPARISON BETWEEN i_{qT0} AND i'_{qT0} FOR THE TWO PM-SYR (EXP).

Motor	Mot_1	Mot_2
$T_{\mathrm{PM}}/T_{\mathrm{n}}$ **(%)**	11.2	34.2
i_{nom} **(Apk)**	28	22.2
i_{qT0} **(A)**	-2.36	-7.59
i'_{qT0} **(A)**	-2.30	-8.25
ϵ_{T0} **(%)**	-0.21	3.0

B. Methods for Extracting i'_{qT0}

Based on (16), an elliptic current trajectory is expected, with the major axis aligned with the q axis. So, as a first attempt, the incremental saliency was evaluated as the ratio between the maximum HF current elongation in d and q axes, called Δi_d and Δi_q respectively:

$$\xi_{dq} = \frac{\Delta i_\mathrm{q}}{\Delta i_\mathrm{d}} \tag{17}$$

Following this approach, the red curve of Fig. 11 was obtained for Mot_1. As can be seen, this method resulted unreliable for determining i'_{qT0}. So, a different strategy is proposed here.

In reality, the current ellipse is slightly rotated respect to the dq axes, as summarized in Fig. 10, where the major and minor axes of the ellipse are not aligned with dq coordinates. This reminds the rotation caused by cross-saturarion effect, which should be absent in this region being $i_\mathrm{d} = 0$. To determine the local saliency of the machine, irrespectively of the axes rotation, the ratio between major and minor axes of the current ellipse is adopted:

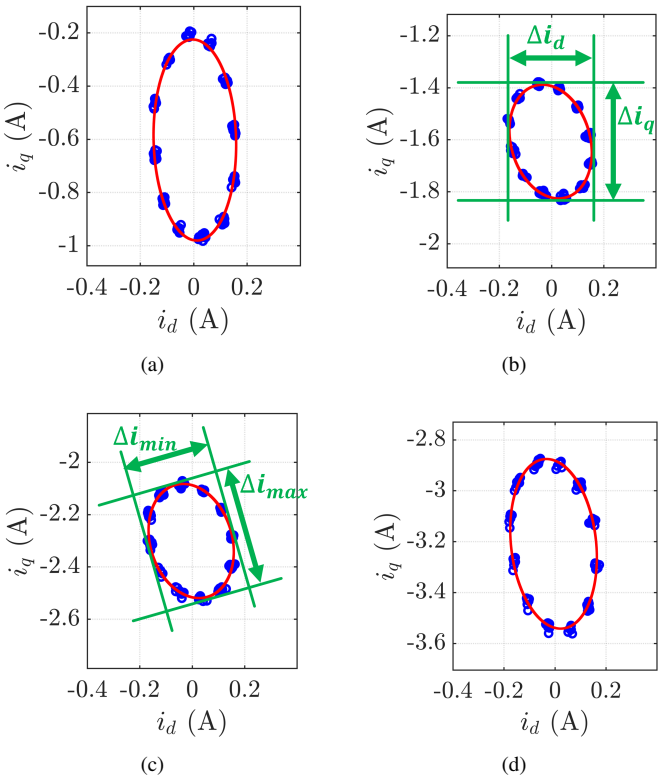

(a) (b) (c) (d)

Fig. 10. Saliency analysis along the q-axis with a HF rotating voltage superimposed to a DC excitation of (a) $i_\mathrm{q} = -0.6$ A, (b) $i_\mathrm{q} = -1.6$ A (c) $i_\mathrm{q} = -2.3$ A (d) $i_\mathrm{q} = -3.2$ A. Blue: measurement points. Red: fitting curve. Machine: Mot_1.

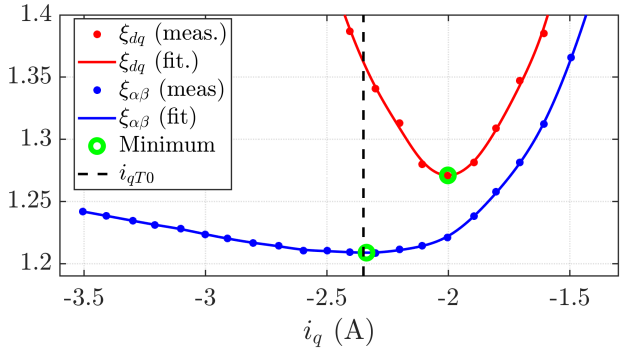

Fig. 11. Evaluated saliency along q-axis with (blue) or without (red) considering ellipse rotation. Black dashed line: reference i_{qT0}. Motor: Mot_1.

$$\xi_{\alpha\beta} = \frac{\Delta i_{max}}{\Delta i_{min}} \tag{18}$$

In this way, the ellipse rotation is compensated finding the real machine local saliency.

Dealing with the causes of the misalignment, the effect of stator resistance, neglected in (16), would produce a small tilt of the ellipse. Also, a non-perfect operation of the BSF of in Fig. 9 would deviate the HF voltage vector and thus the current response. Upon verification, both effects resulted negligible in the adopted experimental test bench. Altogether, an error in sensorless position estimate is retained the most probable justification of this non-ideality, and will be object of further experimental verification. The use of (14) compensates for any of such effects, and results in an accurate estimate of the current value i'_{qT0} for all the motors under test.

As can be seen in Table II, in each case the measured i'_{qT0} results very close to i_{qT0}. For the Mot_1, the saliency variation with i_{q} is represented with the blue line in Fig. 11.

Finally, λ_{pm} is evaluated based on (14). The results are summarized in Table II. As can be seen, a very good accuracy is reached for every tested motor. The obtained $\lambda_{\mathrm{q}}(i_{\mathrm{q}})$ characteristics for the two prototypes are reported in Fig. 12.

C. Sensitivity Respect to the HF Test Voltage

For the sake of evaluating the dependency of the λ_{pm} estimation respect to the HF voltage amplitude, the test was repeated on varying u_{c} from 5 to 25 V with steps of 5 V. In every set of tests, summarized in Table III, the estimation of λ_{pm} resulted very accurate. For the prototype Mot_1, the absolute relative error is lower than 2 % in the worst case. Slightly higher discrepancy is obtained for Mot_2, but still lower than 4 %. To evaluate the impact of this variability, Fig. 12(b) shows the estimated $\lambda_{\mathrm{q}}(i_{\mathrm{q}})$ characteristic obtained with the best (-0.12 % error) and the worst (3.99 %) λ_{pm} estimation, in blue and green line respectively. As can be seen, both the characteristics are practically overlapped with the reference trajectory (red line).

VII. Conclusion

The main contribution of this work is the evaluation of λ_{pm} at standstill and without necessity of position transducers.

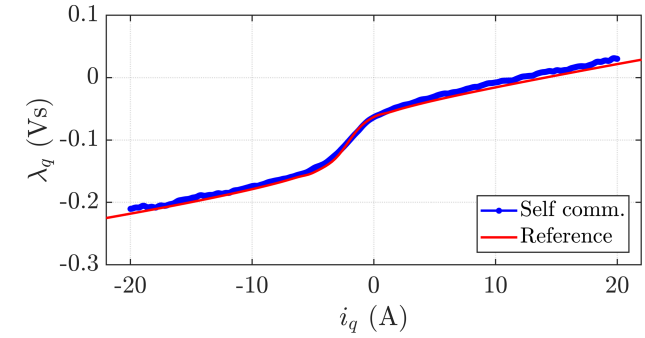

(a)

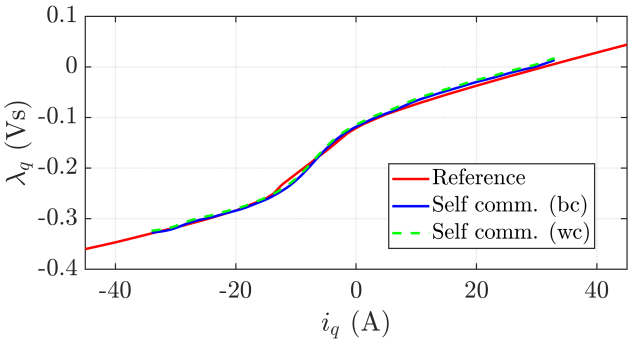

(b)

Fig. 12. Final $\lambda_{\mathrm{q}}(i_{\mathrm{q}})$ characteristic obtained from stand-still self-commissioning for the machine (a) Mot_1 and (b) Mot_2. In (b), the blue line is obtained estimating i'_{qT0} with an injection of u_{c}=10 V (best case, error of -0.12% on λ_{pm} estimation), while the green dashed line refers to u_{c}=15 V (worst case, error of 3.99%).

TABLE III
Sensitivity of λ_{pm} evaluation respect to the amplitude of the injected voltage.

u_{c} (V)	measured i'_{qT0} (A)		λ_{pm} error (%)	
	Mot_1	Mot_2	Mot_1	Mot_2
5	-2.395	-8.586	1.33	-3.60
10	-2.335	-8.255	-0.50	0.61
15	-2.389	-7.928	1.24	3.99
20	-2.337	-8.105	-0.42	-0.12
25	-2.119	-8.091	1.82	2.28

The proposed technique relies on machine local anisotropy along negative q axis, evaluated through HF excitation test and proper post-processing manipulation. A deep analysis of the machine conditions during the test is carried out to clearly understand the related magnetic phenomena. This test completes the standstill self-commissioning procedure [22] extending the results to PM-SyR machines. Overall, the complete flux maps of PM-SyR machines are retrieved at standstill, without locking the rotor and encoderless. A block diagram of the proposed test sequence is reported in Fig. 13. Accurate experimental results were obtained on two PM-SyR prototypes with different ratings.

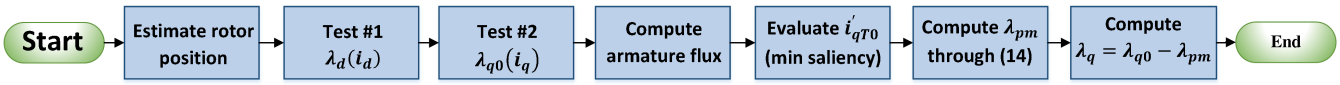

Fig. 13. Block diagram of the proposed standstill self-commissioning test sequence.

APPENDIX: EQUIVALENCE BETWEEN i_{qT0} AND i'_{qT0}

A. Physical Explanation

To better understand the correlation between minimum saliency and zero torque locus, an intuitive way is to consider an equivalent SyR machine. Fig. 14(a) reports in red the $\lambda_{\mathrm{q}}(i_{\mathrm{q}})$ characteristic of a typical SyR motor. As widely known, this curve is symmetric for positive and negative i_{q}, and it presents an inflection point with maximum slope (and so maximum l_{q}) at $i_{\mathrm{q}} = 0$. The blue curve in the same Figure represents the $\lambda_{\mathrm{q}}(i_{\mathrm{q}})$ characteristic of the same machine when PM are added into the flux barriers, thus obtaining a PM-SyR motor, without modifying the machine geometry. As can be seen, the two lines present almost the same shape, but the second one is shifted down and left. Both these effects are due to the PM.

Figure 14(b) compares the torque contour of the same machines (SyR and PM-SyR) in the dq plane. As can be seen, the SyR machine (red contour in the left sub-figure) presents null torque along d- and q-axes, while in each quadrant the iso-torque lines are symmetrical and almost following hyperbolic functions. Also in this case the shape of the torque lines in the PM-SyR case (blue-right sub-figure) is almost the same, but it is slightly shifted down vertically. The two trajectories of null torque are now the q-axis and the ZTL, which cross each other in the point $(i_{\mathrm{d}}, i_{\mathrm{q}}) = (0, i_{\mathrm{qT0}})$.

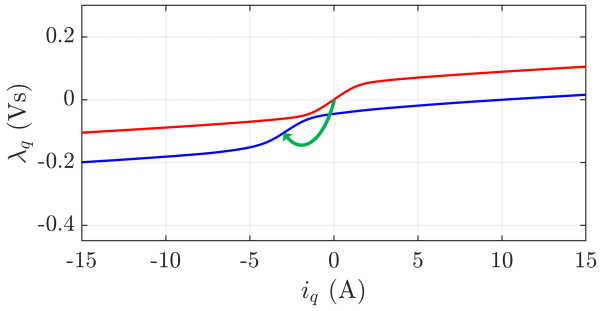

(a)

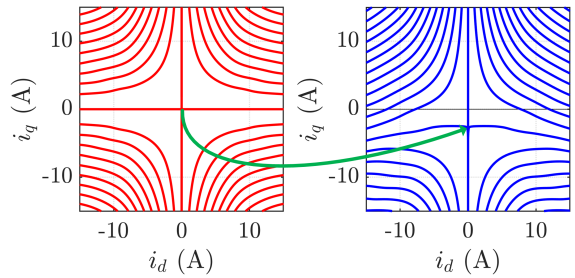

(b)

Fig. 14. Effect of the PM on (a) $\lambda_{\mathrm{q}}(i_{\mathrm{q}})$ and (b) $T(i_{\mathrm{d}} i_{\mathrm{q}})$ based on the model of Mot_2^a. Red: SyR; blue: PM-SyR; green arrows: PM effect.

It must be noted that in the SyR case the two trajectories at $T = 0$ cross in the origin of the plane, thus for $i_{\mathrm{q}} = 0$, where the l_{q} is maximum. The assumption $i_{\mathrm{qT0}} \approx i'_{\mathrm{qT0}}$ is thus supported if we consider the PM having equal effect on the $\lambda_{\mathrm{q}}(i_{\mathrm{q}})$ and $T(i_{\mathrm{d}}, i_{\mathrm{q}})$ characteristics. This is generally true at least in the case the PM-SyR machine is not too far from optimal design criteria. In any case, it must be noted that an approximation is introduced.

B. FEA Analysis

A deep FEA analysis was carried out to verify the correspondence between i_{qT0} and i'_{qT0}. In particular, the Finite Element Models (FEM) of four machines were considered. For each of them, the values of i_{qT0} and i'_{qT0} were retrieved and compared. The results are summarized in Table IV.

At first, the model of one of the prototypes under test (Mot_2) was considered. This motor is designed with three flux barriers, so it presents high anisotropy. Anyway, roughly 34.2% of the rated torque T_{n} is generated by the PMs insert into the rotor barriers (T_{PM}). This means the amount of PMs is quite high respect to classical PM-SyR machines, as for example Mot_1. This improves the motor torque density, even if it goes to the detriment of the field weakening capability.

A modification of the same motor was considered, called Mot_2^a, where the PM remanence was virtually reduced by 50%. As a consequence, only 10.4% of the torque is due to the PM. Conversely, no additional tests were carried out increasing the PM strength, since the prototype already presents high levels of induction, and eventual increased PM field would cause rotor saturation at no load.

A further case is analyzed, called Mot_2^b, where the radial ribs of the Mot_2 machine were increased by 20%, keeping the same amount of PM. This is meant to emulate a motor designed for higher speed, so that the ribs must ensure higher mechanical robustness. Because of the higher flux necessary to saturate the structural ribs, the PM torque is slightly decreased respect to the Mot_2 case. No modifications were made on the reference stator, therefore the three machines Mot_2, Mot_2^a and Mot_2^b present the same rated current.

TABLE IV
COMPARISON BETWEEN i_{qT0} AND i'_{qT0} FOR DIFFERENT PM-SYR (FEA).

Motor	Mot_2	Mot_2^a	Mot_2^b	Mot_3
$T_{\mathrm{PM}}/T_{\mathrm{n}}$ **(%)**	34.2	10.4	30.7	53.7
i_{nom} **(Apk)**	22.2	22.2	22.2	120
i_{qT0} **(A)**	-5.47	-2.52	-5.39	-39.2
i'_{qT0} **(A)**	-5.31	-2.72	-5.81	-39.4
ϵ_{T0} **(%)**	-0.73	0.91	1.90	0.20
$\epsilon_{\lambda_{\mathrm{pm}}}$ **(%)**	-1.91	-0.71	3.96	-0.48

At last, the model of a high anisotropy PMSM adopted in commercial electric vehicles (Toyota Prius 2010) was considered, called Mot_3. This motor presents much higher rated power and also higher percentage of PM torque (53.7%).

As can be seen in Table IV, in every analyzed motor the approximation $i_{\mathrm{qT0}} \approx i'_{\mathrm{qT0}}$ is reasonably good. The discrepancy is evaluated as:

$$\epsilon_{\mathrm{T0}} = \frac{i_{\mathrm{qT0}} - i'_{\mathrm{qT0}}}{i_{\mathrm{nom}}} \tag{19}$$

For each considered model, an estimation of PM flux linkage $\hat{\lambda}_{\mathrm{pm}}$ was retrieved based on i'_{qT0} and (14). The error respect to λ_{pm} is computed as:

$$\epsilon_{\lambda_{\mathrm{pm}}} = \frac{\lambda_{\mathrm{pm}} - \hat{\lambda}_{\mathrm{pm}}}{\lambda_{\mathrm{pm}}} \tag{20}$$

A good λ_{pm} estimate is reached for each analyzed case. Slightly higher inaccuracy is observed for the motor Mot_2^b, explained because in this motor a relevant part of the PM flux is necessary to saturate the ribs at no load. Anyway, also in this case, the discrepancy is lower than 4%, which is acceptable for most of the applications requiring self-commissioning tests.

ACKNOWLEDGMENT

The research has been conducted with the support of Power Electronics Innovation Center (PEIC) of Politecnico di Torino.

REFERENCES

[1] F. Briz and M. W. Degner. Rotor position estimation. IEEE Industrial Electronics Magazine, June 2011.

[2] J. M. Liu and Z. Q. Zhu. Novel sensorless control strategy with injection of high-frequency pulsating carrier signal into stationary reference frame. IEEE Transactions on Industry Applications, July 2014.

[3] W. T. Villet, M. J. Kamper, P. Landsmann, and R. Kennel. "Evaluation of a simpli
ed high frequency injection position sensorless control method for reluctance synchronous machine drives," in *6th IET International Conference on Power Electronics, Machines and Drives (PEMD 2012)*, March 2012.

[4] N. Bianchi, E. Fornasiero, M. Ferrari and M. Castiello, "Experimental Comparison of PM-Assisted Synchronous Reluctance Motors," in *IEEE Transactions on Industry Applications*, vol. 52, no. 1, pp. 163-171, Jan.-Feb. 2016.

[5] A. Vagati, M. Pastorelli, F. Scapino and G. Franceschini, "Impact of cross saturation in synchronous reluctance motors of the transverse-laminated type," in *IEEE Transactions on Industry Applications*, vol. 36, no. 4, pp. 1039-1046, July-Aug. 2000.

[6] N. Bianchi, E. Fornasiero and S. Bolognani, "Effect of Stator and Rotor Saturation on Sensorless Rotor Position Detection," in *IEEE Transactions on Industry Applications*, vol. 49, no. 3, pp. 1333-1342, May-June 2013.

[7] L. Ortombina, E. Liegmann, P. Karamanakos, F. Tinazzi, M. Zigliotto and R. Kennel, "Constrained Long-Horizon Direct Model Predictive Control for Synchronous Reluctance Motor Drives," 2018 IEEE 19th Workshop on Control and Modeling for Power Electronics (COMPEL), Padua, 2018, pp. 1-8

[8] Y. Lee and S. Sul, "Model-Based Sensorless Control of an IPMSM With Enhanced Robustness Against Load Disturbances Based on Position and Speed Estimator Using a Speed Error," in *IEEE Transactions on Industry Applications*, vol. 54, no. 2, pp. 1448-1459, March-April 2018.

[9] A. Favato, P. G. Carlet, F. Toso and S. Bolognani, "A Model Predictive Control for Synchronous Motor Drive with Integral Action," IECON 2018 - 44th Annual Conference of the IEEE Industrial Electronics Society, Washington, DC, 2018, pp. 325-330.

[10] D. Paulus, P. Landsmann and R. Kennel, "Sensorless field- oriented control for permanent magnet synchronous machines with an arbitrary injection scheme and direct angle calculation," 2011 Symposium on Sensorless Control for Electrical Drives, Birmingham, 2011, pp. 41-46.

[11] L. Rovere, A. Formentini, A. Gaeta, P. Zanchetta and M. Marchesoni, "Sensorless Finite-Control Set Model Predictive Control for IPMSM Drives," in *IEEE Transactions on Industrial Electronics*, vol. 63, no. 9, pp. 5921-5931, Sept. 2016.

[12] A. Varatharajan, P. Pescetto and G. Pellegrino, "Sensorless Synchronous Reluctance Motor Drives: A Full-Speed Scheme using Finite-Control-Set MPC in a Projection Vector Framework," in *IEEE Transactions on Industry Applications*, 2020.

[13] S. Ichikawa, M. Tomita, S. Doki and S. Okuma, "Sensorless Control of Synchronous Reluctance Motors Based on Extended EMF Models Considering Magnetic Saturation With Online Parameter Identification," in IEEE Transactions on Industry Applications, vol. 42, no. 5, pp. 1264-1274, Sept.-Oct. 2006.

[14] IEEE, "1812-2014 - IEEE Trial-Use Guide for Testing Permanent Magnet Machines.", 2015.

[15] E. Armando, R. I. Bojoi, P. Guglielmi, G. Pellegrino and M. Pastorelli, "Experimental Identification of the Magnetic Model of Synchronous Machines," in *IEEE Transactions on Industry Applications*, vol. 49, no. 5, pp. 2116-2125, Sept.-Oct. 2013

[16] S. A. Odhano, P. Pescetto, H. A. A. Awan, M. Hinkkanen, G. Pellegrino and R. Bojoi, "Parameter Identification and Self-Commissioning in AC Motor Drives: A Technology Status Review," in *IEEE Transactions on Power Electronics*, vol. 34, no. 4, pp. 3603-3614, April 2019

[17] S. Yang and K. Lin, "Automatic Control Loop Tuning for Permanent-Magnet AC Servo Motor Drives," in *IEEE Transactions on Industrial Electronics*, vol. 63, no. 3, pp. 1499-1506, March 2016.

[18] A. Accetta, M. Cirrincione, M. Pucci and A. Sferlazza, "A Saturation Model of the Synchronous Reluctance Motor and its Identification by Genetic Algorithms," *2018 IEEE Energy Conversion Congress and Exposition (ECCE)*, Portland, OR, 2018, pp. 4460-4465.

[19] S. De Caro, S. Foti, T. Scimone, A. Testa, L. D. Tornello and G. Scelba, "A New Self-Commissioning Technique for Sensorless Synchronous Reluctance Motor Drives," 2019 IEEE 10th International Symposium on Sensorless Control for Electrical Drives (SLED), Turin, Italy, 2019, pp. 1-6.

[20] L. Peretti, P. Sandulescu and G. Zanuso, "Self-commissioning of flux linkage curves of synchronous reluctance machines in quasi-standstill condition," in *IET Electric Power Applications*, vol. 9, no. 9, pp. 642-651, 11 2015.

[21] N. Bedetti, S. Calligaro and R. Petrella, "Stand-Still Self-Identification of Flux Characteristics for Synchronous Reluctance Machines Using Novel Saturation Approximating Function and Multiple Linear Regression," in *IEEE Transactions on Industry Applications*, vol. 52, no. 4, pp. 3083-3092, July-Aug. 2016.

[22] M. Hinkkanen, P. Pescetto, E. Mölsä, S. E. Saarakkala, G. Pellegrino and R. Bojoi, "Sensorless Self-Commissioning of Synchronous Reluctance Motors at Standstill Without Rotor Locking," in *IEEE Transactions on Industry Applications*, vol. 53, no. 3, pp. 2120-2129, May-June 2017.

[23] P. Pescetto and G. Pellegrino, "Automatic Tuning for Sensorless Commissioning of Synchronous Reluctance Machines Augmented With High-Frequency Voltage Injection," in *IEEE Transactions on Industry Applications*, vol. 54, no. 5, pp. 4485-4493, Sept.-Oct. 2018.

[24] M. Hinkkanen, S. E. Saarakkala, H. A. A. Awan, E. Mölsä and T. Tuovinen, "Observers for Sensorless Synchronous Motor Drives: Framework for Design and Analysis," in *IEEE Transactions on Industry Applications*, vol. 54, no. 6, pp. 6090-6100, Nov.-Dec. 2018.

[25] J. Holtz. "Acquisition of position error and magnet polarity for sensorless control of pm synchronous machines", in IEEE Transactions on Industry Applications, July 2008.

[26] T. Tuovinen, H. A. Ali Awan, J. Kukkola, S. E. Saarakkala and M. Hinkkanen, "Permanent-Magnet Flux Adaptation for Sensorless Synchronous Motor Drives," 2018 *IEEE 9th International Symposium on Sensorless Control for Electrical Drives (SLED)*, Helsinki, 2018, pp. 138-143.

[27] Z. Q. Zhu, X. Zhu, P. D. Sun and D. Howe, "Estimation of Winding Resistance and PM Flux-Linkage in Brushless AC Machines by Reduced-Order Extended Kalman Filter," 2007 *IEEE International Conference on Networking, Sensing and Control*, London, 2007, pp. 740-745.

[28] S. A. Odhano, P. Giangrande, R. I. Bojoi and C. Gerada, "Self-Commissioning of Interior Permanent- Magnet Synchronous Motor Drives With High-Frequency Current Injection," in *IEEE Transactions on Industry Applications*, vol. 50, no. 5, pp. 3295-3303, Sept.-Oct. 2014.

[29] P. Pescetto and G. Pellegrino, "Sensorless magnetic model and pm flux identification of synchronous drives at standstill," *2017 IEEE International Symposium on Sensorless Control for Electrical Drives (SLED)*, Catania, 2017, pp. 79-84.

[30] J. Jacob, P. Kumar, S. Calligaro and R. Petrella, "Self-Commissioning Identification of Permanent Magnet Flux-Linkage Magnitude in Sensorless Drives for PMSM at Quasi Stand-Still," *2018 IEEE 9th International Symposium on Sensorless Control for Electrical Drives (SLED)*, Helsinki, 2018, pp. 144-149.
[31] P. Pescetto and G. Pellegrino, "Standstill Determination of PM Flux Linkage Based on Minimum Saliency Tracking for PM-SyR Machines," *2019 IEEE Energy Conversion Congress and Exposition (ECCE), Baltimore, MD*.

PLACE PHOTO HERE

Paolo Pescetto received the B.Sc. and M.Sc. degrees with full grade and honors from Politecnico di Torino, Turin, Italy, in 2013 and 2015. Since 2015 he worked in the same institution toward the PhD degree obtained "Cum Laudem" in 2019. Since fall 2019 he is working as researcher in the Energy Department of Politecnico di Torino. He is a member of the Power Electronics Innovation Center (PEIC) of Politecnico di Torino. In 2014 he was an Erasmus Student at the Norwegian University of Science and Technology, Trondheim. He authored or co-authored 10 IEEE journal papers. His main research interests include synchronous motor drives, sensorless control, self-commissioning techniques and integrated battery chargers for EVs. Dr. Pescetto received three Paper Awards in the IEEE conferences and one PELS PhD thesis award.

PLACE PHOTO HERE

Gianmario Pellegrino (M'06 – SM'13) received the MSc and PhD degrees in electrical engineering from Politecnico di Torino, Turin, Italy in 1998 and 2002, respectively. He is currently a Professor of Electrical Machines and Drives at the same university. Dr. Pellegrino is engaged in several research projects with the industry, and one of the authors of the open-source project SyR-e for the design of electrical motors. He was a visiting fellow at Aalborg University, Denmark, the University of Nottingham, UK, and the University of Wisconsin-Madison, USA. Dr. Pellegrino is an Associate Editor for the IEEE Transactions on Industry Applications and an IEEE Senior Member. He has 50+ IEEE journal papers, three patents and seven Best Paper Awards. He is a member of the Power Electronics Interdepartmental Laboratory (PEIC) of Politecnico di Torino and a member of the Advisory Board of PCIM Europe. He is currently the Secretary of the CMAEL Association, representative of the scholars in Power Converters, Electrical Machines and Drives in Italy, and the Rector's Advisor for Interdepartmental Centers of Politecnico di Torino.